Suppression of energetic particle driven instabilities with HHFW heating

2015 Nucl. Fusion 55 013012

(http://iopscience.iop.org/0029-5515/55/1/013012)

IOP Publishing | International Atomic Energy Agency Nuclear Fusion

Nucl. Fusion **55** (2015) 013012 (9pp) doi:10.1088/0029-5515/55/1/013012

Suppression of energetic particle driven instabilities with HHFW heating

E.D. Fredrickson[1], G. Taylor[1], N. Bertelli[1], D.S. Darrow[1], N. Gorelenkov[1], G. Kramer[1], D. Liu[2], N.A. Crocker[3], S. Kubota[3] and R. White[1]

[1] Princeton Plasma Physics Laboratory, Princeton NJ 08543, USA
[2] Department of Physics and Astronomy, University of California, Irvine, CA, USA
[3] Department of Physics and Astronomy, University of California, Los Angeles, CA 90095, USA

E-mail: efredrickson@pppl.gov

Received 28 August 2014, revised 16 October 2014
Accepted for publication 22 October 2014
Published 2 December 2014

Abstract

In plasmas in the National Spherical Torus Experiment (NSTX) (Ono *et al* 2000 *Nucl. Fusion* **40** 557) heated with neutral beams, the beam ions typically excite energetic particle modes (or fishbones), and toroidal, global or compressional Alfvén eigenmodes. These modes can redistribute the energetic beam ions, altering the beam driven current profile and the plasma heating profile, or they may affect electron thermal transport or cause losses of the beam ions. In this paper we present experimental results where these instabilities, driven by the super-thermal beam ions, are suppressed with the application of high harmonic fast wave heating.

Keywords: toroidal Alfvén eigenmode, high harmonic fast wave heating, global Alfvén eigenmode

(Some figures may appear in colour only in the online journal)

1. Introduction

Many methods, ranging from plasma shaping [1] or application of non-axisymmetric fields [2] to using RF heating to directly affect the fast-ion distribution [3], have been proposed or observed to modify fast-particle-driven instabilities. In previous experiments on NSTX [3], high harmonic fast wave (HHFW) heating at 30 MHz was used in an attempt to increase fast-ion phase-space diffusivity through heating of the energetic beam ions, thereby suppressing the chirping of toroidal Alfvén eigenmodes (TAEs). Some success was achieved in the suppression of chirping of the higher frequency global Alfvén eigenmodes (GAEs) and there was suggestive evidence that HHFW could suppress the TAE under some circumstances (see figures 8 and 9, [3]). Here we report on experiments [4] where not only the TAE but also GAE and fishbone activity was suppressed with higher power HHFW. In these experiments, typically more HHFW power was applied, for longer intervals, than in the previous experiments. Additionally, the target plasma had significantly lower plasma current. What is particularly interesting about these experiments is that the TAEs are excited through a broad range of resonances [5, 6], the GAE through a Doppler-shifted cyclotron resonance [7, 8] and the fishbones through precession drift or bounce resonance [9, 10], yet the HHFW apparently suppressed all of these instabilities.

2. Experimental results

In this experiment there are 13 shots with various combinations of HHFW and NBI heating including one shot with only 2 MW of NBI heating, no HHFW (figures 1(*a*) and 2(*a*)). The other 12 shots all had 2 MW of NBI with between 1.5 and 3 MW of HHFW heating. There were also a number of shots with 1.5 to 2 MW of HHFW heating and no beams, thus no beam-ion-driven modes. All shots were helium target plasmas with a toroidal field of 3.8 kG, and a plasma current of 0.3 MA. This was not an experiment dedicated to TAE stabilization and in this dataset the HHFW antenna phasing has been varied.

In figure 1 spectrograms from two similar NSTX shots are shown, both with 2 MW of neutral beam heating from 0.15 to 0.6 s. The first two panels of figure 1 compare spectrograms covering the GAE frequency range for a shot with (*a*) only NBI and, (*b*) with 3 MW of HHFW and 2 MW of NBI heating. GAE activity is seen shortly after beam injection starts for both shots, but is suppressed during the HHFW heating in the second shot. The GAE activity returns in the second shot following the cessation of HHFW heating.

Spectrograms for the TAE and fishbone frequency ranges are shown in panels (*a*) and (*b*) of figure 2. Again, TAE are present for both shots prior to the HHFW heating, but both

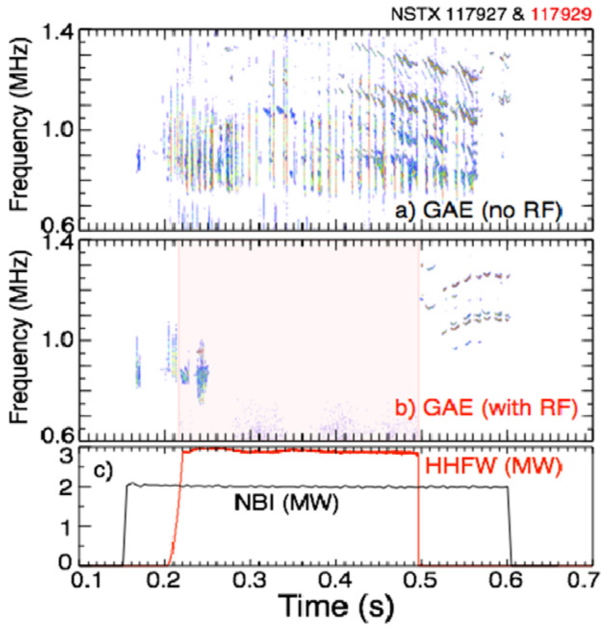

Figure 1. Spectrograms showing GAE frequency range: (*a*) w/o RF, (*b*) GAE frequency range with RF, (*c*) NBI and HHFW (30 MHz) power waveforms.

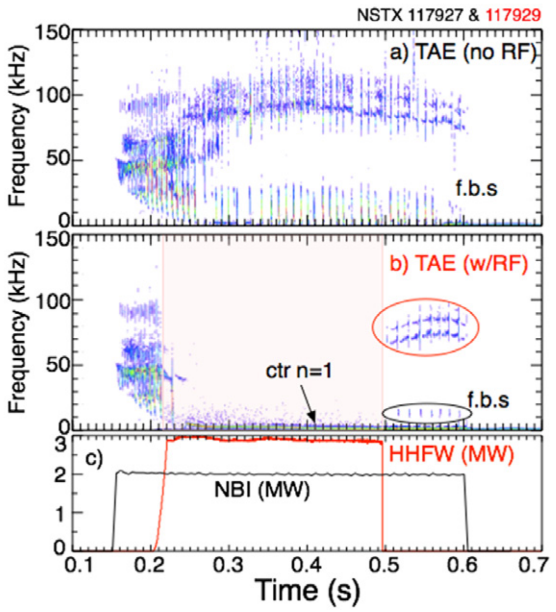

Figure 2. Spectrograms showing TAE frequency range: (*a*) w/o RF, (*b*) TAE frequency range with RF, (*c*) NBI and HHFW power waveforms.

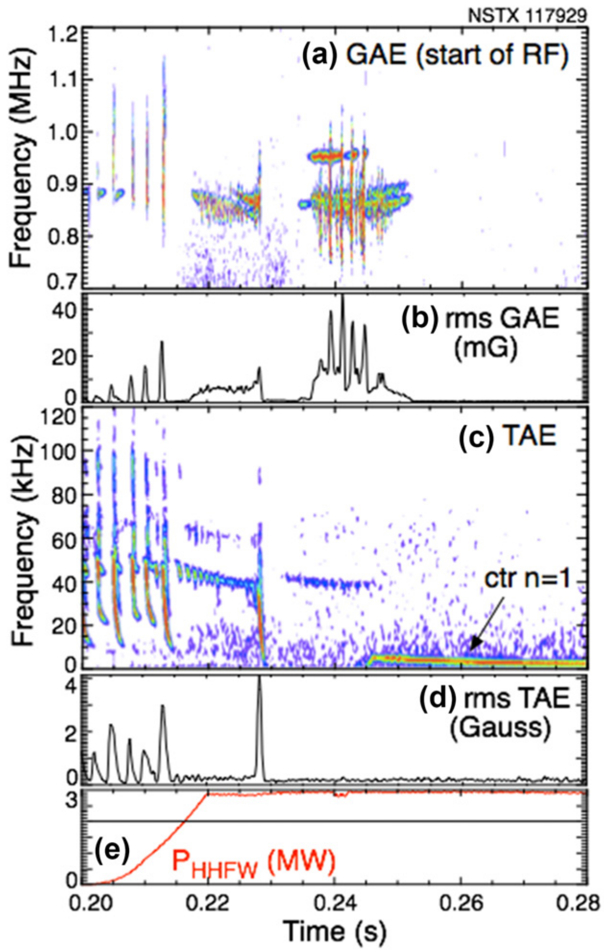

Figure 3. (*a*) Spectrogram showing suppression of GAE with HHFW heating, (*b*) rms GAE fluctuation level (0.7–1.1 MHz), (*c*) spectrogram covering TAE frequency range, (*d*) rms TAE fluctuation level (10–120 kHz), (*e*) evolution of source HHFW power.

TAE and fishbones are suppressed during the HHFW heating pulse (pink shaded area). The TAE and fishbones reappear after the end of the HHFW heating. The fishbones are weaker following the HHFW in the second shot than in the same time range in the beam-only shot.

The timescales for mode suppression after HHFW onset and for the modes to recover following HHFW heating could provide information on the mechanism of mode suppression. If we expand the spectrograms from figures 1 and 2 around the start of HHFW heating (figure 3), it is seen that both the GAE and TAE activity persist for 40 to 50 ms after the start of HHFW heating. The strong frequency chirping of both the TAE and GAE appear to be quickly suppressed, although in both cases, frequency chirps do reappear. The delay in suppression after the start of HHFW heating then suggests that it either takes some time to modify the fast-ion distribution responsible for exciting the TAE and GAE, or there was some change in the equilibrium plasma parameters during this interval which affected the stability of the Alfvénic modes.

Expanding the spectrograms about the end of HHFW heating, both the TAE and GAE reappear within a few ms of the end of HHFW (figure 4). This is much shorter than the fast-ion slowing-down time, suggesting that the perturbation to the fast-ion distribution was relatively small, and/or that the HHFW in some way directly interfered with the resonant interaction of the fast ions with the mode. The TAE appear to begin avalanching shortly after their reappearance and the peak amplitude of the bursts is comparable to that in the beam-only shot. The TAE avalanches are correlated with a weak fishbone-like mode. The reappearance of the TAE and GAE argues against an explanation that these discharges were evolving towards equilibrium conditions where the TAE and GAE were intrinsically stable.

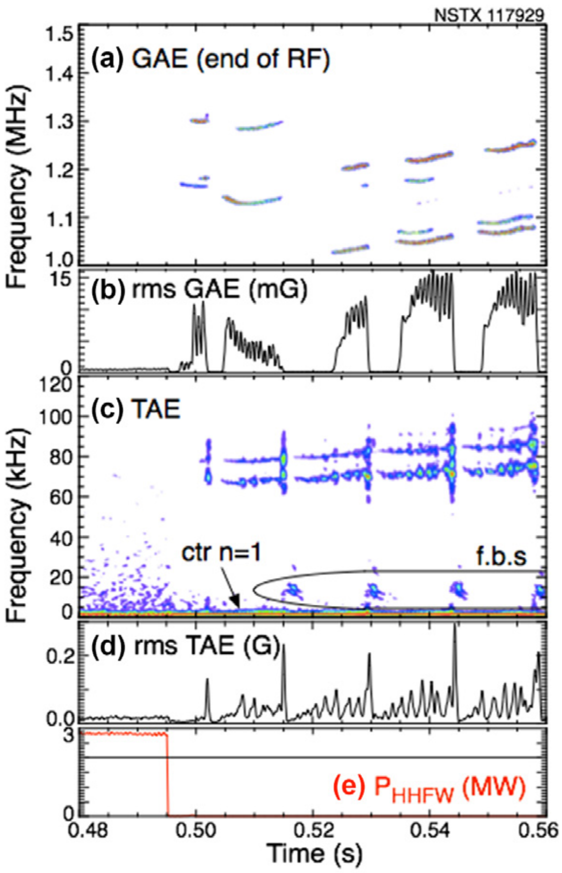

Figure 4. (*a*) Spectrogram showing suppression of GAE with HHFW heating, (*b*) rms GAE fluctuation level (0.9–1.4 MHz), (*c*) spectrogram covering TAE frequency range, (*d*) rms TAE fluctuation level (60–120k kHz), (*e*) evolution of source HHFW power (red), beam power (black).

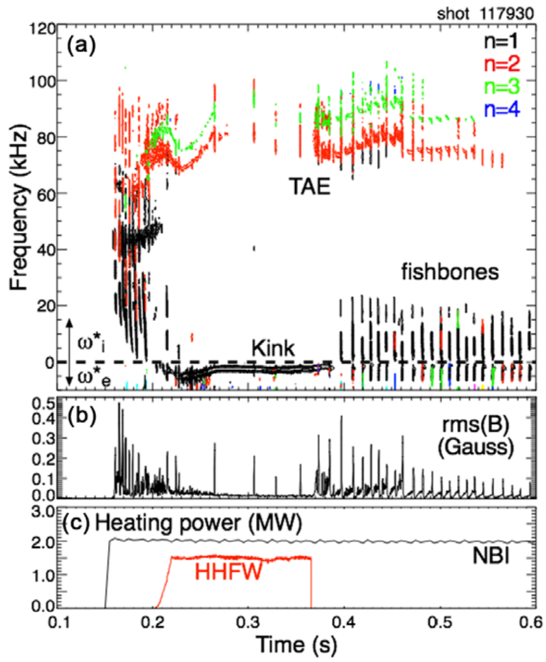

Figure 5. (*a*) Spectrogram showing partial suppression of TAE with 1.5 MW of HHFW power, (*b*) rms magnetic fluctuation level 60–100 kHz. TAE and fishbones recover after the end of HHFW heating.

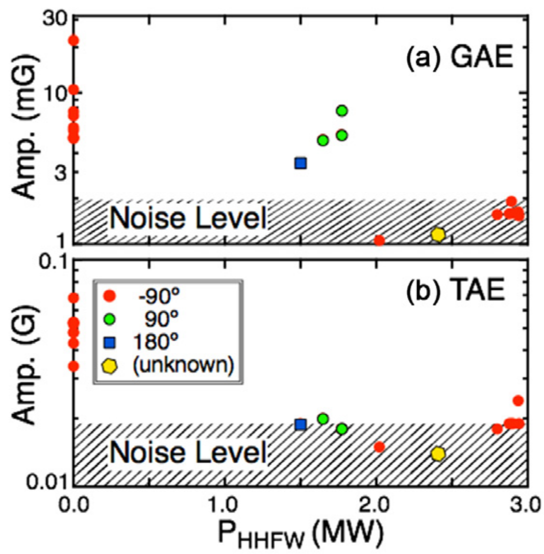

Figure 6. Rms fluctuation level: (*a*) 0.6–1.4 MHz (GAE) and (*b*) 60–100 kHz (TAE) versus HHFW power. Colours indicated antenna strap phasing.

The threshold power for stabilization for the parameters in this experiment is about 1.5 MW of HHFW for the 2 MW of NBI used in these shots. In figure 5 a shot with 2 MW of NBI is shown during which a shorter, 1.5 MW pulse of HHFW is applied. As can be seen in figure 5(*a*), the TAE activity is reduced, but not completely suppressed during the HHFW pulse, and returns shortly after the end of HHFW heating. The TAE amplitude following the HHFW is comparable to that in the pre-HHFW pulse.

In figure 3(*c*) an $n = 1$ mode appears at about the same time the TAE and GAE are completely suppressed. An $n = 1$ counter-propagating kink mode is commonly observed during HHFW heating, and often persists after HHFW heating ends (see figures 3(*c*), 4(*c*) and 5(*a*)). In figure 4(*c*) weaker fishbones co-exist with the counter-propagating $n = 1$ kink mode and it is possible that the kink is at least partially responsible for the suppression of the fishbones. In figure 5(*a*) the kink persists for ≈25 ms after the end of the HHFW, coexisting with the strong TAE bursts, but the fishbone activity does not return until the kink is gone. The TAE activity co-exists with the $n = 1$ kink at lower HHFW power, as in figure 5(*a*), so it is not believed that the $n = 1$ is responsible for suppressing the TAE or GAE, as is seen more clearly in figure 5.

In figure 6 the rms fluctuation levels are shown for TAE and GAE activity against the average HHFW power (all shots here had 2 MW of NBI heating). The rms fluctuation level for points with HHFW power is averaged over the HHFW heating period, excluding the first 50 ms, as suppression is typically delayed by up to 50 ms. The no-HHFW power points all follow the HHFW heating period. Initial beam-heating periods before HHFW heating were excluded as the q-profile had typically not relaxed, and TAE activity was qualitatively different. The HHFW power shown here is the

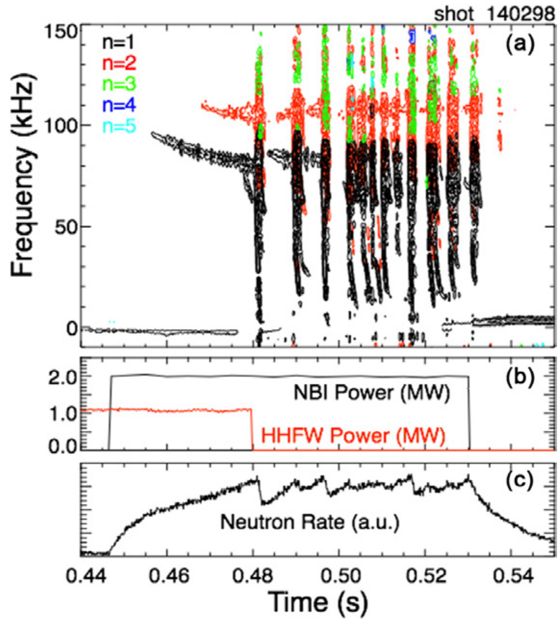

Figure 7. (*a*) Spectrogram of magnetic fluctuations showing TAE and TAE avalanche activity, (*b*) waveforms of NBI (black) and HHFW power (red), (*c*) neutron rate with drops at TAE avalanche events.

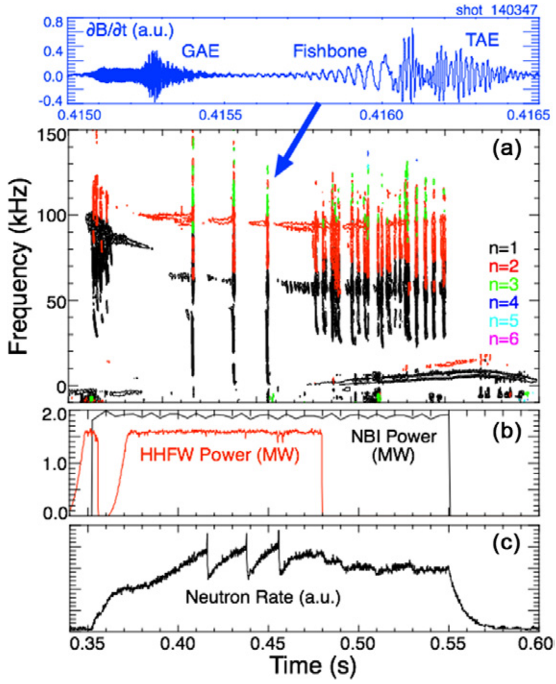

Figure 8. (*a*) Spectrogram of magnetic fluctuations showing TAE and TAE avalanche activity, (*b*) waveforms of NBI (black) and HHFW power (red), (*c*) neutron rate with drops at TAE avalanche events.

source power, and is not necessarily the power coupled to the plasma. Under some conditions significant power loss to the scrape-off layer is seen [11–13], which may have a dependence on antenna phasing. The colours of the points in figure 6 indicate the phasing between antenna straps. There is no, however, sufficient data from this experiment to determine if there is a dependence of the effect on antenna phasing.

A later experiment, again at low current and plasma density but with deuterium target plasmas, also found some indications of TAE suppression by HHFW heating. In figure 7 the spectrogram from a 300 kA is shown, low-density plasma heated with 2 MW of NBI and 1 MW of HHFW. The toroidal field in this case was higher than the previous examples, 4.65 kG versus 3.8 kG. In this case an ≈80 ms NBI pulse was added towards the end of an HHFW heating period, with about 30 ms of overlap. While TAE activity is not completely suppressed, the strong avalanches begin coincident with the end of the HHFW pulse. This shot had only 1 MW of HHFW heating power, but the lower density or higher field may have improved the efficacy of the beam-ion heating by the HHFW power.

A similar shot with somewhat higher HHFW source power did not see complete suppression of the TAE avalanches (figure 8). However, in this case the behaviour was somewhat more complex. During the HHFW pulse there were three strong bursts of multiple-mode (GAE/TAE/fishbone) activity, but again, regular TAE avalanching begins coincident with the end of HHFW heating. Close inspection each of the three TAE avalanche events during the HHFW pulse reveals that they were initiated by a GAE, which triggered fishbone activity [14, 15] and the fishbone, in turn, triggered the TAE avalanche (figure 8(*a*)), the reverse of the more common situation where the TAE avalanches trigger the fishbones [15–17]. This shot was also a 300 kA, 4.65 kG plasma, but at ≈20% higher density ($n_e(0) \approx 2 \times 10^{13}$ cm^{-3} versus 1.6×10^{13} cm^{-3}).

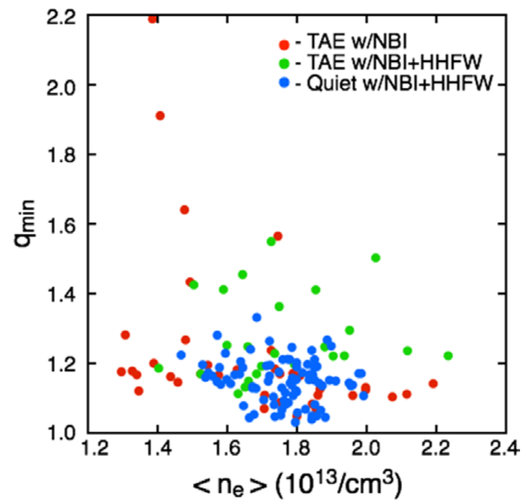

Figure 9. Line-averaged electron density and q_{min} averaged over 25 ms intervals from 12 discharges. Red points are conditions with TAE and NBI, but no HHFW, green TAE with NBI and HHFW, blue are quiet with NBI and HHFW.

Possible correlations of thermal plasma parameters with TAE presence were looked for by constructing a database of plasma parameters in each 25 ms interval of the plasmas in this experiment. In figure 9 the average density and the q_{min} for each of the 25 ms intervals are shown. The red points correspond to intervals where TAEs were present with beams, but no HHFW heating. The green points are intervals where TAEs were present with beam and HHFW heating, mostly time intervals just after the start of HHFW heating, or intervals with lower HHFW power (1.5 to 2 MW). Finally, the blue points are intervals where TAE activity is absent, despite 2 MW of NBI

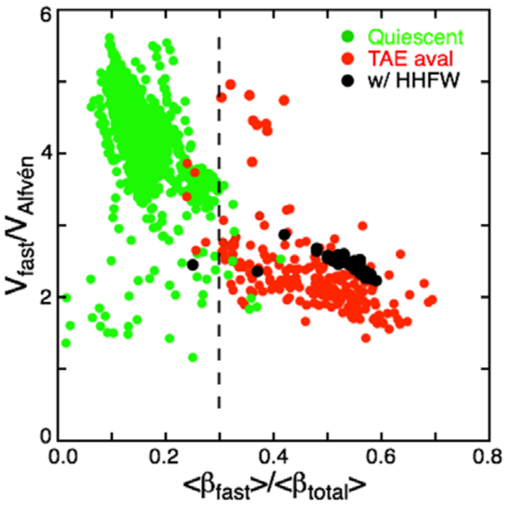

Figure 10. Parameters for quiescent (green) and TAE avalanching (red) NBI heated plasmas. The HHFW-stabilized parameters are shown in black.

heating, presumably suppressed by the HHFW heating. The TAE-quiescent parameters of electron density q_{min} (as well as electron temperature, not shown) overlap the parameter ranges for shots where TAEs were present with only NBI heating.

The normalized parameters $\beta_{fast}/\beta_{total}$ and $V_{fast}/V_{Alfvén}$ are found to be reasonable predictors for the occurrence of avalanching TAE activity or TAE-quiescent plasmas on NSTX [18]. The HHFW-stabilized TAE-quiescent beam-heated plasma parameters are compared with the TAE stability map for NSTX in figure 10. Here, the HHFW-quiescent points are shown as black circles, overlaid on the broader, beam-heating only database from NSTX. In this figure, parameters of plasmas with TAE avalanches are shown as red circles, and those with quiescent plasmas are shown as green circles. Previous studies [18] of TAE activity scaling had found that TAE-quiescent beam-heated plasmas were only found when the ratio of β_{fast} to β_{total} was less than $\approx$0.3 (green points, figure 10). The quiescent plasmas from this experiment, however, largely overlap the TAE avalanching region from NBI-only NSTX plasmas.

3. Simulation of fast-ion losses from TAE avalanches

In previous work it has been reported that reasonable agreement is found between measured mode amplitudes and mode amplitudes needed to predict neutron drops consistent with experimental measurements [19, 20]. The predictions use eigenmode structures from the NOVA ideal code [21–23] in the guiding-centre orbit following code ORBIT [24]. A similar analysis was carried out for a TAE avalanche at 0.23 s in the beam-only shot (figure 11). Only one reflectometer channel [25] was available for internal measurement of the mode amplitude, and that channel's reflection layer was near the magnetic axis, so the mode amplitude was not as well constrained as in previous studies (figure 11(*b*), red points). The ideal stability code, NOVA, is used to find the TAEs, using equilibrium parameters. The $n = 1$ eigenmode, combined with the measured electron density profile, is used to simulate

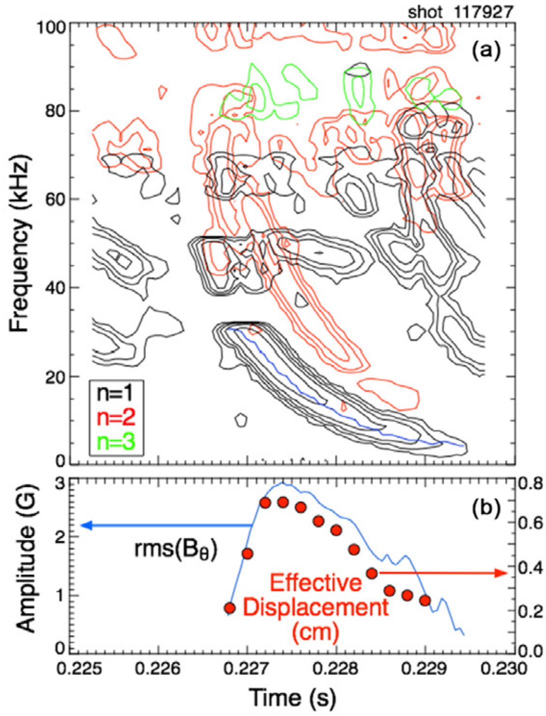

Figure 11. (*a*) Spectrogram showing TAE avalanche consisting of $n = 1$ and $n = 2$ TAE, (*b*) amplitude evolution for $n = 1$ measured with a single reflectometer channel (red points) and from the Mirnov coil (blue line).

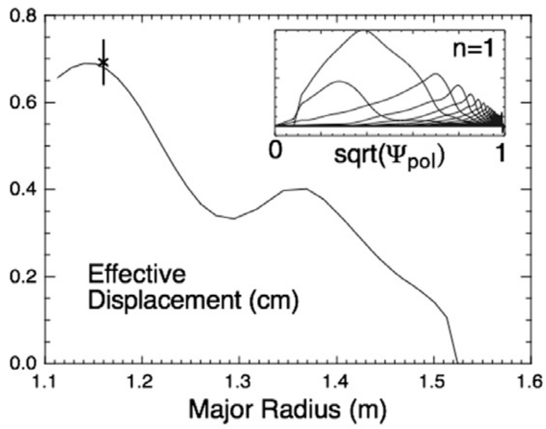

Figure 12. Simulated reflectometer array response for $n = 1$ mode (solid line) and effective displacement from a single reflectometer channel (black point). Inset shows NOVA poloidal harmonics for the modes.

the radial profile of the effective displacement as would be measured with a reflectometer array. In figure 12 the simulated reflectometer profile is scaled to the single measurement.

The eigenfunctions from NOVA together with the experimental amplitude and frequency evolution in time of the $n = 1$ and $n = 2$ largest modes are used in the ORBIT code to model the change in the fast-ion distribution through this TAE burst. Using the eigenfunctions normalized to the reflectometer measurement of the mode amplitude evolution overestimates the measured neutron rate drop. In figure 13 the calculated neutron rate change through the TAE avalanche as a

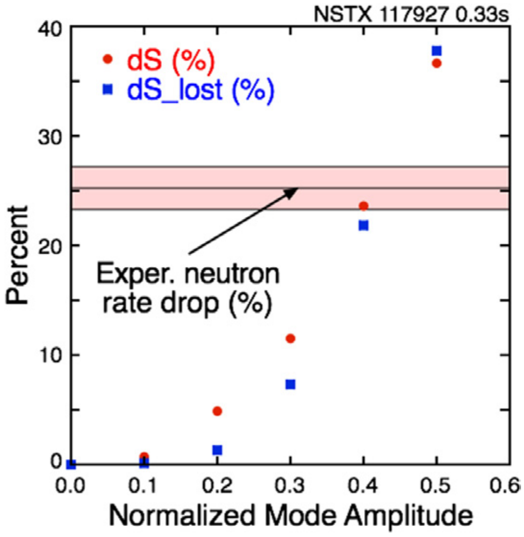

Figure 13. Neutron rate drop calculated with the ORBIT code as a function of normalized input mode amplitude.

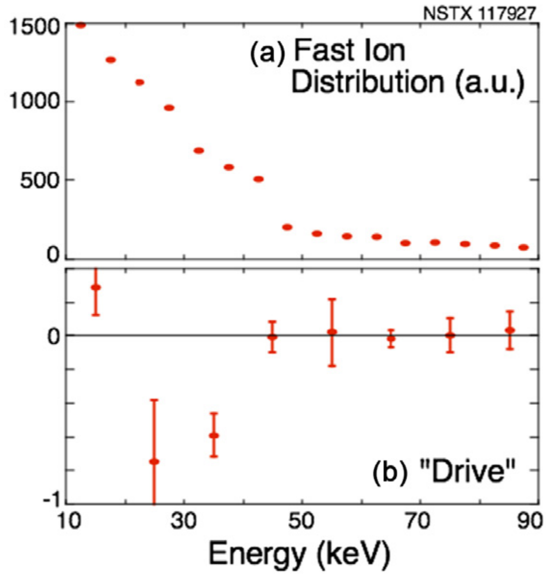

Figure 14. (*a*) Fast-ion distribution input to ORBIT, (*b*) change in energy of fast ions in bin versus energy.

function of peak mode amplitude normalized to the measured amplitude is shown. Here it is found that the calculated neutron drop at a mode amplitude of ≈40% of the measured mode amplitude is in reasonable agreement with the experimental measurement. The target plasma for these experiments was helium, so the neutron production calculated in TRANSP [26] with the NUBEAM beam deposition code [27] was mostly beam–beam (87%) with a relatively small amount of beam–target (≈13%). Thermal neutron production was negligible. In contrast to previous analysis of avalanches in higher current H-mode plasmas, the bulk of the neutron drop here is predicted to be from fast-ion losses.

3.1. TAE drive

The ORBIT code can also be used to study the resonant drive of the TAE. Simulations with ORBIT are run as above, but with amplitudes scaled from the nominal mode amplitude by a factor of 0.4% to 1% to make the result as close to a linear response as possible. By looking at the energy change for different ranges of the initial fast-ion energy, it is found that the bulk of the drive for the TAE comes from fast ions with energies below 40 keV. In figure 14(*a*) the fast-ion slowing-down distribution calculated in TRANSP and used in ORBIT is shown. Figure 14(*b*) shows that fast ions with energies between 20 and 40 keV have contributed the most energy to the TAE. The fast ions with energies above 40 keV contribute little net drive within the statistical uncertainty although these more energetic fast ions can interact strongly with the TAE. The error bars are found from multiple ORBIT runs with mode amplitude normalized from 0.4% to 1% of the peak measured amplitude.

The only diagnostics on NSTX measuring the confined fast ions for these experiments were the neutral particle analysers (NPAs) and neutron detectors. In figure 15 data from one of the four solid state NPA (ssNPA) chords [28] are shown. This chord samples predominantly parallel going fast ions. There are small differences between the NPA signals during HHFW and beam-only shots. As plasma and beam parameters

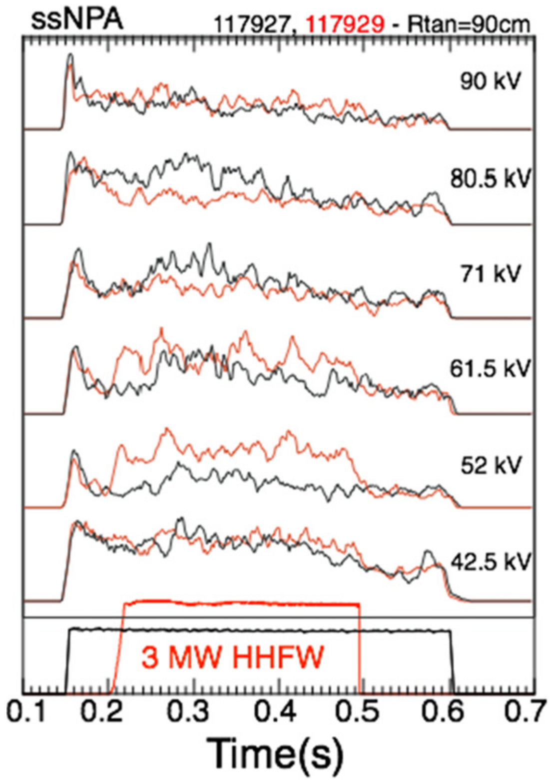

Figure 15. ssNPA data for energy channels comparing shot with HHFW heating (red) and without (black). This chord with tangency radius of 90 cm views predominantly co-going fast ions.

were very similar between these shots, the measurements indicate that the fast-ion population driving the TAE is not considerably changed in the HHFW shots, although it cannot be ruled out that the effect of the TAE on the fast ions in the beam-only shot might be similar to that of the HHFW. These data are an indication only that the HHFW is not strongly affecting the fast-ion distribution driving the TAE, as the ssNPA

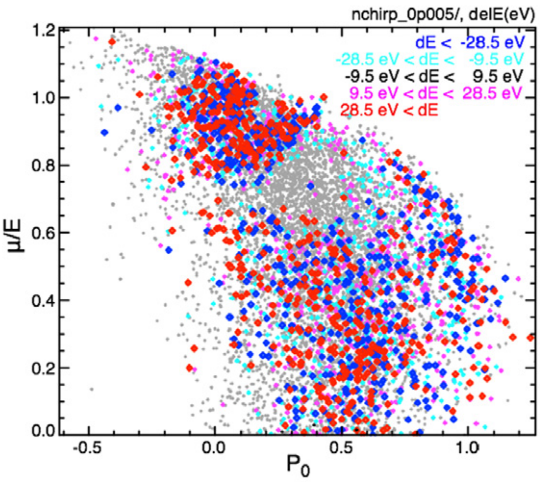

Figure 16. Fast-ion distribution used in ORBIT simulations. Colours indicate change in energy of each fast ion through a very small amplitude (0.5% of nominal peak amplitude) simulation.

only measures down to ≈40 keV, which from figure 14 is still above the energy of fast ions most responsible for driving the TAE. Simulations of the effect of HHFW on the fast-ion population under different conditions show some heating [3] or fast-ion redistribution and loss [29].

In figure 16 the fast-ion distribution in normalized-μ versus canonical angular momentum (P_0) space is shown. Each point represents the initial position of a beam fast ion and the colour of the point indicates whether the ion gained or lost energy to the mode. The points in red indicate fast ions that lost the most energy, and in blue, those that gained the most energy. At the end of the simulation, there was a net loss of energy (albeit, very small) from the total fast-ion distribution, indicating that the fast ions had given energy to the modes. The resonant fast ions (those with large energy changes) are distributed fairly isotropically throughout the initial distribution, with the exception of the 'gap' for $\approx 0.6 < \mu/E <\approx 0.8$ and $P_0 >\approx 0.2$. Gross distortions of the distribution function in this space seem unlikely to strongly influence the mode drive. However, other representations of the distribution function, as yet undiscovered, might.

4. Stability calculations

The modelling of the effect of the HHFW heating on the fast-ion population will be addressed in a future publication. However, we can qualitatively examine the impact of some broad changes to the fast-ion distribution on the TAE stability. It is still important to understand whether the suppression of EPM, TAE and the higher frequency AE is coincidental, or reflect some broader, possibly more direct, mechanism applicable to all three forms of beam-ion-driven instabilities. Previous HHFW modelling, albeit for different plasma conditions, has found that HHFW heats the beam-ion distribution. It might be assumed also that HHFW heating adds primarily perpendicular energy to the beam ions. Motivated by these assumptions, the NOVA-k stability calculations are performed for a small scan in the initial pitch angle of the beam-ion population, and in the maximum energy.

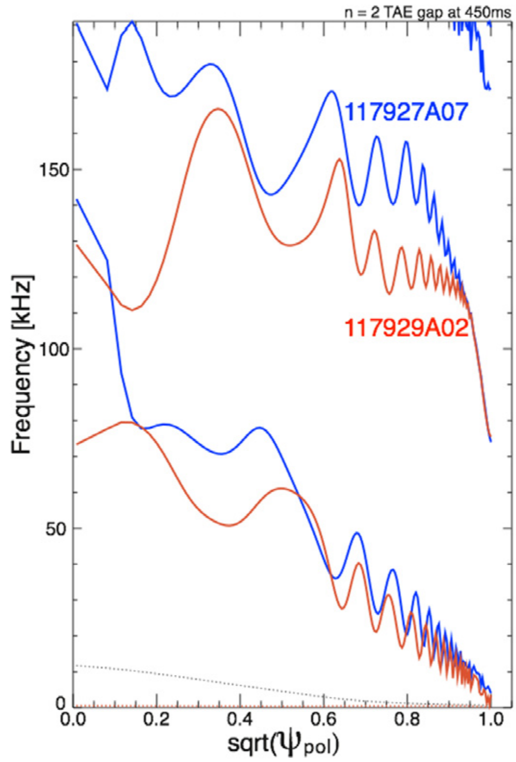

Figure 17. The NOVA calculation of the $n = 2$ continuum for the two shots shown in figure 2 at 0.45 s.

In figure 17 is a representative comparison of the continuum plots at 0.45 s for the two shots shown in figure 2. The equilibrium parameters are very similar; however, there are some minor differences in the shape of the q-profile near the axis (where the uncertainties are fairly large). Additionally, the beam-only shot has some small toroidal rotation velocity whereas the beam + HHFW shot has nearly zero rotation. The NOVA-k calculations of TAE growth rates, in terms of a model fast-ion slowing-down distribution find some evidence that lower pitch-angle distribution (more perpendicular, as expected from HHFW heating), give a lower drive. Also, a more energetic fast-ion distribution (again, as might be expected from HHFW heating of the beam ions) also reduces the growth rates. While these results might be suggestive, much further work is planned towards modelling of the HHFW heating effect on the fast-ion distribution.

At present, NOVA-k uses a parametrized slowing-down (or Maxwellian) distribution for the fast ions which cannot accurately reflect more general modifications of the fast-ion distribution by RF heating. Future work is envisioned to include HHFW wavefield calculations with TORIC or AORSA, combined with CQL3D or SPIRAL to calculate the perturbation to the fast-ion distribution. The perturbed fast-ion distribution may then be used in ORBIT, SPIRAL or a new version of NOVA-k to evaluate the impact on TAE stability. New experiments with the improved fast-ion diagnostics expected for NSTX-U (tangential and perpendicular FIDA, and the NPA diagnostics) will provide data on the perturbations to the fast-ion distribution to be compared with CQL3D or SPIRAL predictions.

5. Summary

In this paper we have presented for the first time experimental results where multiple instabilities driven by the super-thermal beam ions are seen to be suppressed with the application of high harmonic fast wave heating. Toroidal Alfvén eigenmodes, global Alfvén eigenmodes and fishbones were all suppressed, even though the resonant drive mechanisms for these classes of modes are very different. The experiments described here are with relatively low plasma current (300 kA), relatively low density and with neutral beam power of 2 MW. It remains for future experiments to determine whether this stabilization mechanism can be extended to more typical operational conditions, that is, higher currents, higher densities and more beam power. In these experiments, the modes were reproducibly stabilized for long periods of time. A threshold power of about 1.5 MW was found for stabilization to occur, but that may scale with density and beam power. It seems unlikely that the stabilization was due to massive losses of fast ions with the application of HHFW. The ssNPA diagnostic does measure changes in the charge-exchange fast-ion losses, but the changes do not seem consistent with substantial fast-ion losses. The abrupt return of mode activity following HHFW heating suggests that the modifications to the fast-ion distribution were relatively small, or that the HHFW more directly interferes with the resonant drive of the modes.

Direct, experimental evidence for improvement or degradation of fast-ion confinement after application of HHFW is equivocal. The target plasma pre-fill gas is helium, thus the neutron rate could be sensitive to deuterium recycling from the wall, which in turn could be affected by the HHFW. Under some conditions, a fair fraction of the HHFW power can go directly to the scrape-off layer [13]. Heating of the beam ions by HHFW will increase neutron production [3] and beam-ion losses will of course decrease it. In the deuterium shots (at lower HHFW power), and in these helium shots, the neutron rate, which is 87% from beam–beam reactions, was largely unaffected by the HHFW. The signal at some energies increases, and decreases in others, but interpretation of the ssNPA data is complicated. In either case, the change could be due to changes in the radial profile of fast-ion distribution, changes in the energy distribution (e.g. heating), or changes in the charge-exchange process (e.g. neutral density). It is hoped that future experiments with improved diagnostics will obviate the need for speculation in the interpretation of these results.

Acknowledgment

This material is based upon work supported by the US Department of Energy, Office of Science, Contract Number DE-AC02-09CH11466.

References

[1] Testa D. and Fasoli A. 2001 *Nucl. Fusion* **41** 809
[2] Bortolon A., Heidbrink W.W., Kramer G.J., Park J.-K., Fredrickson E.D., Lore J.D. and Podestà M. 2013 Mitigation of Alfvén activity in a tokamak by externally applied static 3D fields *Phys. Rev. Lett.* **110** 265008
[3] Heidbrink W.W. *et al* 2006 *Plasma Phys. Control. Fusion* **48** 1347
[4] Ryan P.M. *et al* 2003 *Plasma Physics and Controlled Fusion Research (Lyon, France, 2002)* (Vienna: IAEA) EX/P2-I3 www-pub.iaea.org/MTCD/publications/PDF/csp_019c/html/node215.htm
[5] Cheng C.Z. and Chance M.S. 1986 *Phys. Fluids* **29** 2471
[6] Breizman B.N., Berk H.L. and Ye H. 1993 Collective transport of alpha particles due to Alfvén wave instability *Phys. Fluids* B **5** 3217
[7] Gorelenkov N.N., Fredrickson E., Belova E., Cheng C.Z., Gates D., Kaye S. and White R. 2003 Theory and observations of high frequency Alfvén eigenmodes in low aspect ratio plasmas *Nucl. Fusion* **43** 228
[8] Belova E., Gorelenkov N.N., Cheng C.Z. and Fredrickson E.D. 2003 Numerical study of instabilities driven by energetic neutral beam Ions in NSTX *Proc. 30th European Physical Society Conf. on Controlled Fusion and Plasma Physics (St Petersburg, Russia, July 2003)* vol 27A (ECA) P-3.102 http://epsppd.epfl.ch/StPetersburg/PDF/P3_102.pdf
[9] McGuire K.M. *et al* 1983 *Phys. Rev. Lett.* **50** 891
[10] Fredrickson E.D., Chen L. and White R.B. 2003 Bounce precession fishbones in the National Spherical Torus Experiment *Nucl. Fusion* **43** 1258
[11] Hosea J. *et al* and the NSTX Team 2008 High harmonic fast wave heating efficiency enhancement and current drive at longer wavelength on the National Spherical Torus Experiment *Phys. Plasmas* **15** 056104
[12] Perkins R.J. *et al* 2013 Fast-wave power flow along SOL field lines in NSTX and the associated power deposition profile across the SOL in front of the antenna *Nucl. Fusion* **53** 083025
[13] Bertelli N. *et al* 2014 Full wave simulations of fast wave heating losses in the scrape-off layer of NSTX and NSTX-U *Nucl. Fusion* **54** 083004
[14] Fredrickson E.D. *et al* 2003 Wave driven fast ion loss in the National Spherical Torus Experiment *Phys. Plasmas* **10** 2852
[15] Fredrickson E.D. *et al* 2012 Observation of global Alfvén eigenmode avalanche events on the National Spherical Torus Experiment *Nucl. Fusion* **52** 043001
[16] Crocker N.A., Peebles W.A., Kubota S., Fredrickson E.D., Kaye S.M., LeBlanc B.P. and Menard J.E. 2006 Three-wave interactions between fast-ion modes in the National Spherical Torus Experiment *Phys. Rev. Lett.* **97** 045002
[17] Podestá M., Bell R.E., Crocker N.A., Fredrickson E.D., Gorelenkov N.N., Heidbrink W.W., Kubota S., LeBlanc B.P. and Yuh H. 2011 Non-linear dynamics of toroidicity-induced Alfvén eigenmodes on the National Spherical Torus Experiment *Nucl. Fusion* **51** 063035
[18] Fredrickson E.D., Gorelenkov N.N., Podesta M., Bortolon A., Gerhardt S.P., Bell R.E., Diallo A. and LeBlanc B. 2014 Parametric dependence of fast-ion transport events on the National Spherical Torus Experiment *Nucl. Fusion* **54** 093007
[19] Fredrickson E.D. *et al* 2013 Fast-ion energy loss during TAE avalanches in the National Spherical Torus Experiment *Nucl. Fusion* **53** 013006
[20] Fredrickson E.D. *et al* 2009 Modeling fast-ion transport during toroidal Alfvén eigenmode avalanches in National Spherical Torus Experiment *Phys. Plasmas* **16** 122505
[21] Cheng C.Z. 1992 *Phys. Rep.* **211** 1–51
[22] Cheng C.Z. 1992 Kinetic extensions of magnethydrodynamic models for axisymmetric toroidal plasmas *Phys. Rep. (Rev. Sec. Phys. Lett.)* **211** 1–51
[23] Kramer G.J. *et al* 2006 Interpretation of core localized Alfvén eigenmodes in DIII-D and Joint European Torus reversed magnetic shear plasmas *Phys. Plasmas* **13** 056104
[24] White R.B. and Chance M.S. 1984 *Phys. Fluids* **27** 2455
[25] Crocker N.A. *et al* 1994 High spatial sampling global mode structure measurements via multichannel

reflectometry in NSTX *Plasma Phys. Control. Fusion* **53** 105001
[26] Budny R.V. 1994 *Nucl. Fusion* **34** 1247
[27] Pankin A. *et al* 2004 *Comput. Phys. Commun.* **159** 157–84
[28] Liu D., Heidbrink W.W., Darrow D.S., Roquemore A.L., Medley S.S. and Shinohara K. 2006 *Rev. Sci. Instrum.* **77** 10F113
[29] Kramer G.J., Budny R.V., Bortolon A., Fredrickson E.D., Fu G.Y., Heidbrink W.W., Nazikian R., Valeo E. and Van Zeeland M.A. 2013 A description of the full-particle-orbit-following SPIRAL code for simulating fast-ion experiments in tokamaks *Plasma Phys. Control. Fusion* **55** 025013